Charge separation and transport in conjugated-polymer/semiconductor-nanocrystal composites studied by photoluminescence quenching and photoconductivity

N. C. Greenham,* Xiaogang Peng, and A. P. Alivisatos
Department of Chemistry, University of California, and Molecular Design Institute, Lawrence Berkeley National Laboratory, Berkeley, California 94720
(Received 19 June 1996)

We study the processes of charge separation and transport in composite materials formed by mixing cadmium selenide or cadmium sulfide nanocrystals with the conjugated polymer poly(2-methoxy,5-(2′-ethyl)-hexyloxy-*p*-phenylenevinylene) (MEH-PPV). When the surface of the nanocrystals is treated so as to remove the surface ligand, we find that the polymer photoluminescence is quenched, consistent with rapid charge separation at the polymer/nanocrystal interface. Transmission electron microscopy of these quantum-dot/conjugated-polymer composites shows clear evidence for phase segregation with length scales in the range 10–200 nm, providing a large area of interface for charge separation to occur. Thin-film photovoltaic devices using the composite materials show quantum efficiencies that are significantly improved over those for pure polymer devices, consistent with improved charge separation. At high concentrations of nanocrystals, where both the nanocrystal and polymer components provide continuous pathways to the electrodes, we find quantum efficiencies of up to 12%. We describe a simple model to explain the recombination in these devices, and show how the absorption, charge separation, and transport properties of the composites can be controlled by changing the size, material, and surface ligands of the nanocrystals.
[S0163-1829(96)03048-2]

I. INTRODUCTION

Composites of organic polymers and inorganic nanocrystals are particularly interesting materials in the study of electrical transport. The band gaps and offsets of typical semiconducting polymers and nanocrystals are such that charges will separate across an interface between them. This paper explores the extent of such charge separation, and the nature of charge transport in polymer/nanocrystal blends.

Electronic processes in conjugated polymers are currently the subject of intensive study, both because of fundamental interest in the nature of the electronic excitations in these ''one-dimensional'' semiconductors, and because they have potential applications in a range of electronic devices such as light-emitting diodes.[1–3] Conjugated polymers have the advantage of being easy to process to form large-area devices, and their energy gap and ionization potential can readily be tuned by chemical modification of the polymer chain.[4,5] Large-area thin-film photovoltaic devices based on conjugated polymers are also of interest, although devices fabricated using a single layer of polymer have been found to have low efficiencies of conversion of incident photons to electrons.[6–9] Efficient collection of charge carriers requires that the neutral excited states (singlet excitons) produced by photoexcitation be separated into free charge carriers, and that these carriers are then transported through the device to the electrodes without recombining with oppositely charged carriers. The possibility that conjugated-polymer/nanocrystal composites may have the desired attributes of charge separation and transport motivates the present work.

Charge separation in conjugated polymers has been found to be enhanced at the interface with a material of higher electron affinity where it is energetically favorable for the electron to transfer onto the second material. Examples of such materials include C_{60},[10–13] cyano-substituted conjugated polymers,[14,15] and various small organic molecules.[16] Since the diffusion range of singlet excitons in conjugated polymers is typically in the range 5–15 nm,[13,17–19] it is necessary to have a large area of interface between the two materials in order to achieve a high quantum efficiency for charge separation. Furthermore, the charge separation process must be fast compared to the radiative and nonradiative decays of the singlet exciton, which typically occur with time constants in the range 100–1000 ps. In composite materials where charge separation can occur, the photoluminescence is found to be strongly quenched, since the singlet exciton is no longer able to decay radiatively to the ground state. In the absence of an electric field to remove the separated charges, there must exist a nonradiative process by which recombination occurs between electron and hole on adjacent materials. Although this process is not well understood, it is likely to be much slower than the decay of the singlet exciton. The lifetime of the charge-separated species in composites of poly(2-methoxy,5-(2′-ethyl-hexyloxy)-*p*-phenylenevinylene) (MEH-PPV) with C_{60} has been estimated to be of the order of milliseconds at 80 K.[20] The problem of transport of carriers to the electrodes without recombination is a more difficult one to solve, since it requires that once the electrons and holes are separated onto different materials, each carrier type has a pathway to the appropriate electrode without needing to pass through a region of the other material. The transport must also be sufficiently fast for the carriers to be removed from the device before significant nonradiative recombination can occur at the interface between the two materials. Encouraging results have been obtained using mixtures of polymers with different electron affinities that phase separate on a length scale

suitable to give effective charge separation whilst providing efficient charge transport to the electrodes.[14,15] Recently, high photovoltaic efficiencies have been reported in C_{60}/MEH-PPV MEH-PPV composites with high C_{60} content.[21] In these composites, derivatization of the C_{60} molecule with a flexible alkyl group has been found to give optimum photovoltaic performance, although the detailed morphology of these composites has not yet been reported.

Nanometer-sized crystals of inorganic semiconductors are another interesting class of low-dimensional materials with useful optical and electronic properties.[22,23] When the size of the nanocrystal is smaller than that of the exciton in the bulk semiconductor, the lowest energy optical transition is significantly increased in energy due to quantum confinement. The absorption and emission energy can thus be tuned by changing the size of the nanocrystal. High-quality samples of nanocrystals of II-VI semiconductors such as CdS and CdSe can now be prepared by chemical methods. The surface of the nanocrystal is typically capped by an organic ligand which ensures solubility and passivates the surface electronically. By changing the size from 6 to 2 nm, the energy gap can be tuned from 2.6 to 3.1 eV in CdS and from 2.0 to 2.6 eV in CdSe.[22,24] The ability to tune the electronic structure of the nanocrystals makes them interesting optical materials; however, making contact to the nanocrystals for electrical measurements is more difficult. Nanocrystal/conjugated-polymer composites offer the prospect of allowing electrical access to the nanocrystals. The electron affinity of CdS and CdSe nanocrystals is in the range 3.8–4.7 eV, hence they are suitable materials to act as electron acceptors when combined with conjugated polymers, where the electron affinity is in the range 2.5–3.0 eV. In contrast to C_{60}, the optical energy gap of these nanocrystals lies conveniently in the visible region, and it is thus possible not only to study electron transfer from polymer to nanocrystal, but also to study hole transfer from nanocrystal to polymer after excitation in the nanocrystal. The nanocrystal surface ligand can be changed without altering the intrinsic electronic properties of the nanocrystal, hence it is possible to control the charge transfer between polymer and nanocrystal, and from nanocrystal to nanocrystal. The surface ligand is also important in determining the morphology of the polymer/nanocrystal composite. Charge separation at the interface between organic molecules and nanocrystals is currently of great interest, particularly since the report by O'Regan and Grätzel of efficient photovoltaic devices based on organic dyes adsorbed on TiO_2 nanocrystalline films.[25] In these devices, the large area of TiO_2 surface allows a high optical density of dye molecules to be achieved, whilst maintaining efficient charge separation. An electrolyte solution is required to remove the holes from the organic dye after charge separation. Charge transfer between CdS nanocrystals and the hole-transporting polymer poly(*N*-vinylcarbazole) has previously been studied; however, the CdS nanocrystals were at low concentration, and acted primarily as a sensitizer, with charge transport occurring through the polymer, rather than from nanocrystal to nanocrystal.[26] Electroluminescence in blends of CdSe nanocrystals and poly(*N*-vinylcarbazole) has been studied by Dabbousi *et al.*[27]

In this paper, we study the photoluminescence and photoconductivity of composite materials formed with MEH-PPV and either CdS or CdSe nanocrystals. The nanocrystals may either be in direct contact with the polymer, or, alternatively, the surface of each nanocrystal may be coated with a surfactant molecule, trioctylphosphineoxide (TOPO), which forms a barrier of 11 Å thickness between the nanocrystal core and the polymer. The structure of MEH-PPV, and schematic diagrams of the TOPO-coated and noncoated nanocrystals are shown in Fig. 1. In polymer/nanocrystal composites when the nanocrystal surface is not coated with TOPO, we find significant quenching of the luminescence, indicating that charge transfer occurs at the polymer/nanocrystal interface. We also study the effect of nanocrystal concentration on the photoconductivity, and find that efficient photoconductivity can be achieved at high nanocrystal concentrations when electrons and holes can be transported, respectively, through the nanocrystal and polymer components of the composite material. Throughout the paper, we support our interpretation of the photophysical measurements with detailed transmission electron microscope (TEM) studies of the morphology of the composite materials.

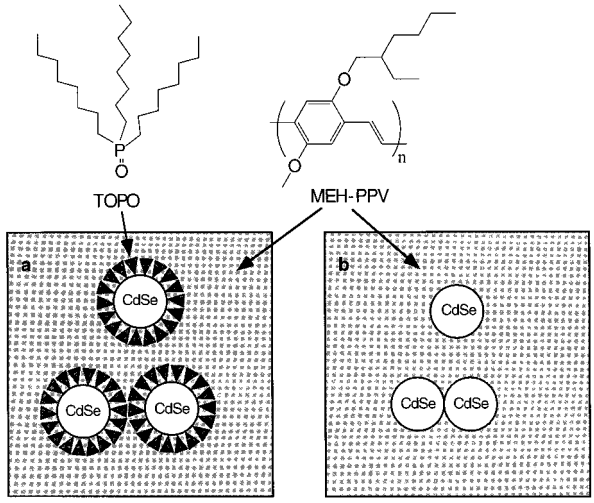

FIG. 1. Schematic diagram of MEH-PPV/nanocrystal composites, showing the chemical structure of MEH-PPV and trioctylphosphineoxide (TOPO). (a) CdSe nanocrystals with surfaces coated by TOPO. (b) CdSe nanocrystals with naked surfaces.

II. EXPERIMENTAL METHODS

MEH-PPV was synthesized by the base-induced polymerization of 2,5-bis(chloromethyl)-1-methoxy-4-(2′-ethyl hexyloxy)benzene in tetrahydrofuran. The product was purified by precipitation with methanol, and was then dissolved in chloroform. CdS and CdSe nanocrystals were synthesized on a gram scale using a modification of a previously reported synthesis.[28,29] A solution of dimethylcadmium and tributylphosphineselenide or bis-trimethylsilanesulfide in tributylphosphine was injected into tri-octylphosphineoxide (TOPO) at 360 °C, followed by heating at 300 °C to give the required size. Full experimental details are given elsewhere.[28,29] The nanocrystals had a good size distribution, with $\sigma<10\%$. In order to prepare samples where the surface TOPO was completely removed, after washing three times in methanol the nanocrystals were three times dissolved in the

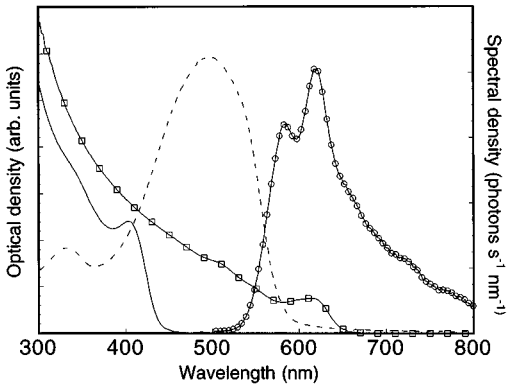

FIG. 2. Absorption spectra of 4-nm-diameter CdS nanocrystals (solid line), 5-nm-diameter CdSe nanocrystals (squares), and MEH-PPV (dashed line). Also shown is the photoluminescence spectrum of MEH-PPV at room temperature, with excitation at 476.1 nm (circles). The nanocrystals were in toluene solution, and the MEH-PPV was a solid film on a glass substrate.

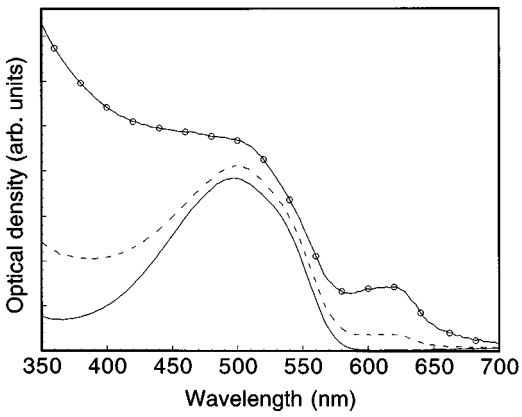

FIG. 3. Absorption spectra of blends of MEH-PPV with 5-nm-diameter CdSe nanocrystals, containing 5% (solid line), 65% (dashed line), and 90% CdSe (circles) by weight.

minimum quantity of pyridine and precipitated by hexanes. The final precipitate was redissolved in chloroform without drying. Concentrations of the polymer and nanocrystal solutions were obtained by evaporating known volumes to dryness and weighing. Thin films were obtained by spin coating from mixed polymer/nanocrystal solutions containing a known ratio of nanocrystal to polymer. Absorption spectra were obtained using a Hewlett Packard 8452A diode array spectrophotometer. Photoluminescence efficiencies of thin films on glass substrates were measured using an integrating sphere, as described elsewhere.[30] Excitation was provided by an argon-ion laser at 476.1 nm with a typical power of 0.1 mW. Transmission electron microscopy (TEM) was performed on very thin films (typically 20 nm) using a JEOL 100-CX microscope operating at 80 kV. TEM samples were prepared by spin coating from dilute solutions onto NaCl substrates. The films were then floated off the NaCl onto the surface of a water bath, and transferred to holey carbon grids.

Photovoltaic devices were prepared by spin coating a film of nanocrystal/MEH-PPV composite onto a glass substrate coated with indium-tin oxide (ITO). Film thicknesses were in the range 300–500 nm. Aluminum electrodes were deposited by vacuum evaporation. The devices were then transferred to a vacuum of approximately 10^{-3} mbar for measurement. Current-voltage curves were measured using a Keithley 928 source-measure unit, both in the dark and under illumination. Monochromatic illumination was provided either by an argon-ion laser, or by the output of a tungsten lamp dispersed by a SPEX 270S monochromator. The spectral resolution of the monochromator system was 3 nm. Spectral responses and quantum efficiencies were determined by normalizing with a calibrated silicon photodiode in the sample position. Quantum efficiencies (electrons/photon) were defined using the total incident flux; reflection losses were neglected.

III. RESULTS

A. Optical properties

Figure 2 shows the absorption spectra of the various nanocrystal and polymer samples used in this work. The emission spectrum of MEH-PPV is also shown. The photoluminescence efficiency for pure MEH-PPV films was found to be in the range 21–24 %, slightly higher than previously reported for this material.[30] Figure 3 shows the absorption spectra of composite films containing 20, 65, and 90 wt % of CdSe. These spectra are simply the sum of the absorption spectra of the constituent parts of the composite films, with no evidence of any additional absorption peaks in the spectral range measured (350–820 nm). These results indicate that there is negligible ground-state charge-transfer between the polymer and the nanocrystals. Also, there is no evidence for any absorption corresponding to a spatially indirect charge-transfer transition between polymer and nanocrystal. Since the absorption coefficient of CdSe nanocrystals is much smaller than that of MEH-PPV, even at the highest concentration of CdSe the optical density of the nanocrystals at their lowest energy absorption peak is smaller than the optical density of the polymer at the π-π^* absorption peak. The film-forming properties of the composite materials were good, and although a small amount of scattering was seen in the most concentrated samples, there was no evidence for gross phase separation on the scale of the wavelength of visible light.

B. Photoluminescence efficiencies

Figures 4(a) and 4(b) show the photoluminescence (PL) efficiency
of nanocrystal/MEH-PPV composites as a function of nanocrystal concentration for cadmium sulfide and cadmium selenide, respectively, with the surface either naked, or coated with TOPO. The easiest case to analyze is that of cadmium sulfide, where the energy gap of the nanocrystals is larger than that of the polymer. With excitation at 476.1 nm, only the polymer is excited, and there is no possibility of exciton transfer from polymer to nanocrystal by Förster transfer. In the case where the nanocrystal surface is covered completely by TOPO, no quenching of the polymer luminescence is observed. This result indicates that electron transfer from polymer to nanocrystal through a layer of TOPO does not occur with rates which compete with the usual radiative and nonradiative decay processes in MEH-PPV. (Typical time constants for singlet exciton decay in MEH-PPV are in

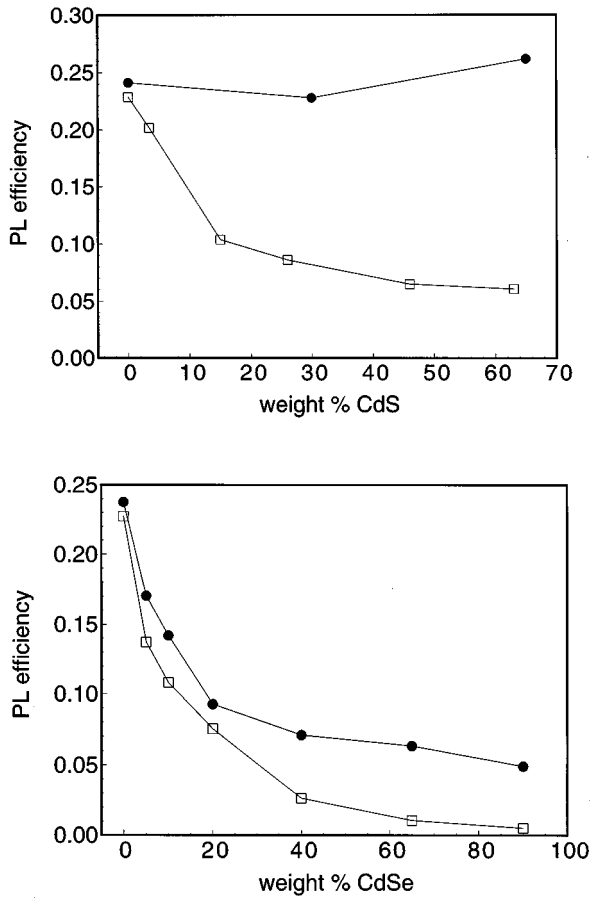

FIG. 4. Photoluminescence efficiency of MEH-PPV/CdSe composites as a function of nanocrystal concentration, for TOPO-coated (circles) and pyridine-treated (squares) nanocrystals. (a) 4-nm-diameter CdS nanocrystals; (b) 5-nm-diameter CdSe nanocrystals.

the range 200–300 ps.[31,32]) Where the surface TOPO is removed by treatment with pyridine, however, there is a significant quenching of the PL, implying that the removal of TOPO allows electron transfer to occur, leading to the formation of separated electron-hole pairs that subsequently recombine nonradiatively. We note that the quenching of the polymer luminescence, whilst substantial, is not complete, even at high nanocrystal concentrations. For pyridine-treated CdS nanocrystals, for example, the PL efficiency levels out at approximately 6% at high concentrations. This suggests the occurrence of phase segregation in the composite materials, since if the nanocrystals were randomly dispersed throughout the sample, we would expect quenching to be much more complete. Similar partial quenching behavior was observed in phase segregated polymer/polymer blends.[14] The subject of phase segregation is discussed in more detail in Sec. III C.

Using CdSe nanocrystals, there is again substantial quenching of the luminescence in the composite materials [Fig. 4(b)]. Except for the case of 90 wt % nanocrystals, excitation at 476.1 nm produces excitation mostly in the polymer, due to the much higher absorption coefficient of MEH-PPV compared with nanocrystals. In contrast to the situation with CdS, it can be seen that for CdSe, quenching occurs even with TOPO-coated nanocrystals, although it is not as effective as with nanocrystals which have been treated with pyridine. With CdSe nanocrystals, there is a good overlap between the polymer emission spectrum and the nanocrystal absorption spectrum, and we therefore expect efficient Förster exciton transfer to occur from polymer to nanocrystal. In contrast to the process of charge transfer, Förster transfer does not require wave-function overlap (tunneling) between the two materials, and can therefore occur in the presence of a TOPO barrier which we have shown above to suppress electron transfer to CdS. The PL quenching observed with TOPO-coated CdSe can therefore be attributed to Förster transfer of the exciton to the nanocrystal, followed by decay with a radiative efficiency significantly less than that of MEH-PPV. The PL spectrum of a composite containing 90 wt % of TOPO-coated CdSe was found to be similar to that of pristine MEH-PPV, indicating that the remaining luminescence comes predominantly from excitons which decay radiatively in the polymer, rather than from excitons which have been created on or transferred onto the nanocrystals. The PL efficiency for these nanocrystals in toluene solution was found to be less than 1%. This low value is consistent with the absence of significant nanocrystal emission compared to the remaining polymer emission.

With pyridine-treated CdSe nanocrystals, the quenching is more effective, suggesting that charge transfer is again taking place. As with CdS, it is energetically favorable for the electron to transfer from polymer to nanocrystal. Alternatively, if the exciton is created on the nanocrystal, or transfers onto the nanocrystal by Förster transfer, the hole can subsequently transfer to the polymer, again producing a charge-separated state with an electron on the nanocrystal and a hole on the polymer. The various electron and exciton transfer processes that can occur using pyridine-treated CdSe are illustrated in Fig. 5. Even with 90 wt % of nanocrystals, the polymer luminescence is not completely quenched. In this composite, 65% of the radiation absorbed at 476.1 nm will directly produce excitons in the nanocrystals, which will decay with low radiative efficiency. The measured PL efficiency of 0.5% therefore corresponds to a radiative efficiency of 1.5% for excitons produced in the polymer. Again, this value is consistent with the occurrence of phase separation. Direct evidence for both electron and hole transfer processes in photovoltaic devices will be presented in Sec. III D. We note that dispersions of nanocrystals in semiconducting polymers, which generally give an alignment of energy levels as shown in Fig. 5, are good for achieving charge separation for photovoltaic applications, but are not ideal for electroluminescence applications, since electrons and holes tend to remain separated on different materials, giving low efficiencies.[27] Devices containing a planar heterojunction between polymer and nanocrystal components can, however, show efficient electroluminescence when the barriers to electron and hole transport at the interface are such as to achieve a good balancing of electron and hole currents.[33]

C. Transmission electron microscopy

Figure 6(a) shows TEM images of blends of MEH-PPV and pyridine-treated CdSe nanocrystals, for various concentrations of nanocrystals. They show the total nanocrystal distribution projected onto the plane of the film. Since the films are thin enough that only a maximum of three to four layers

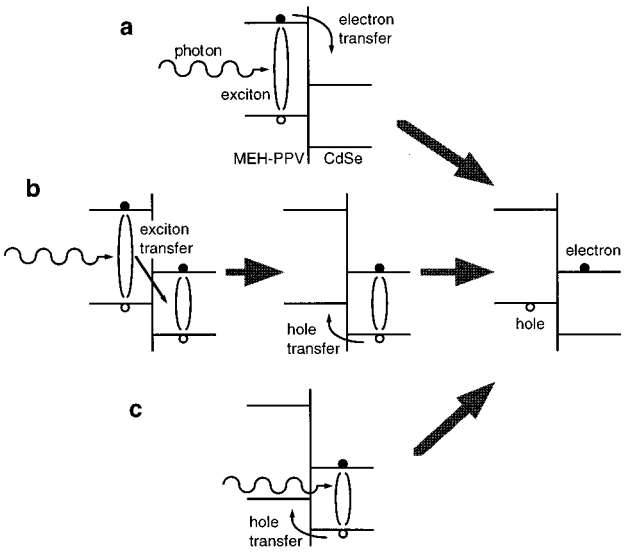

FIG. 5. Routes for exciton and charge transfer in MEH-PPV/CdSe blends. (a) Absorption in the polymer, followed by electron transfer onto the nanocrystal. (b) Absorption in the polymer, followed by exciton transfer onto the nanocrystal, followed by hole transfer onto the polymer. (c) Absorption in the nanocrystal, followed by hole transfer onto the polymer. Note that for CdS nanocrystals, route (b) is not available since the nanocrystal energy gap is larger than that of the polymer, whereas it would be possible for excitons to transfer from nanocrystal to polymer, followed by electron transfer onto the polymer. In the presence of a TOPO barrier, the electron and hole transfer processes are suppressed, and only exciton transfer is possible.

of nanocrystal would be possible, it is easy to resolve the individual nanocrystals. It is clear that, even in dilute blends, the nanocrystals aggregate together to form regions of densely-packed nanocrystals surrounded by regions of polymer which are free from nanocrystals. As the concentration of nanocrystals is increased, the size of the nanocrystal domains increases, and at high concentrations the nanocrystals form a connected network in the plane of the film. At 65 wt % the size of the larger polymer regions is typically 70–120 nm. It should be noted that these images are easy to interpret due to the large difference in scattering between CdSe and MEH-PPV. This contrasts with the situation in polymer/polymer or polymer/C_{60} blends, where it is necessary to dope one of the components selectively in order to achieve contrast in the TEM.[14] The observed morphology is consistent with the substantial but incomplete quenching of the polymer luminescence, given that exciton diffusion ranges in conjugated polymers are estimated to be in the range 5–15 nm.[13,17–19] and that any exciton which reaches a polymer/nanocrystal interface will be quenched. A quantitative comparison is difficult without a more detailed knowledge of the three-dimensional morphology in the thicker films used for the optical measurements. The driving force for phase segregation here is likely to be the difference in polarity between the pyridine-treated nanocrystals, which have polar faces,[34] and the polymer, which is relatively nonpolar.

Figure 6(b) shows TEM images of blends of MEH-PPV and TOPO-coated CdSe nanocrystals, at the same weight percentages of nanocrystals as for the pyridine-coated particles. At the two highest concentrations, there is again clear evidence for aggregation of the nanocrystals, consistent with the PL quenching data. This aggregation is largely driven by van der Waals interactions between the nanocrystals. In this case, the nanocrystal cores within the aggregate are separated by the surface TOPO layers, which appear as light regions in the TEM images. At the lowest concentration, there is almost no aggregation, in contrast to the case where the nanocrystals were treated with pyridine. This improved solubility of the nanocrystals in the polymer is likely to be due to the reduced polarity of the TOPO-coated nanocrystals, and to improved mixing of the flexible alkyl chains of the TOPO molecules with the alkoxy groups of MEH-PPV.

D. Photovoltaic devices

The devices studied comprised a layer of CdSe/MEH-PPV composite between electrodes of ITO and aluminum. For most of the devices, the diameter of the nanocrystals was 5 nm, and the first peak in their absorption spectrum was at 614 nm. The nanocrystals had been treated with pyridine to remove the surface TOPO. Figure 7 shows the current-voltage curve of such a device containing 90 wt % of CdSe, both in the dark, and under monochromatic illumination at 514 nm. The active area of the device was 7.3 mm^2.

Figure 8 shows the short-circuit quantum efficiency (electrons per photon) at 514 nm as a function of nanocrystal concentration, at an excitation intensity of approximately 5 W m^{-2}. For a pure polymer device, the efficiency was only 0.014%, consistent with results reported previously for this kind of device.[14] Adding 5 wt % of nanocrystal gave a factor of 6 improvement in efficiency. Increasing the nanocrystal concentration up to 90 wt % further improved the quantum efficiency to a value of 12%. At -3 V and $+3$ V, this device gave quantum efficiencies of 52% and 71%, respectively. Figure 9 shows the short-circuit current and open-circuit voltage of the device containing 90 wt % of CdSe as a function of incident light intensity. At intensities up to 10 W m^{-2}, the short-circuit current I_{sc} is approximately linear in intensity F with a dependence $I_{sc} \propto F^{0.9}$. At high intensities, the intensity dependence becomes more sublinear, with a dependence $I_{sc} \propto F^{0.65}$. The open circuit voltage shows a much weaker dependence on the intensity, increasing to a value of 0.53 V at an intensity of 500 W m^{-2}.

We have also studied devices containing TOPO-coated nanocrystals of the same core size used in the devices described above. These devices showed extremely low quantum efficiencies, with a value of 0.005% at a loading of 81 wt % nanocrystals.

Figure 10 shows the photoconductivity action spectrum for the same device described in Figs. 7 and 9, along with the action spectrum for a pure MEH-PPV device. The action spectrum of the composite device shows response in the region 600–660 nm where there is no absorption in the polymer. This response corresponds to light which is absorbed in the nanocrystals, with subsequent hole transfer onto the polymer. At wavelengths below 600 nm, the response is due to a combination of absorption in the polymer and in the nanocrystals. The pure MEH-PPV device has a peak in the

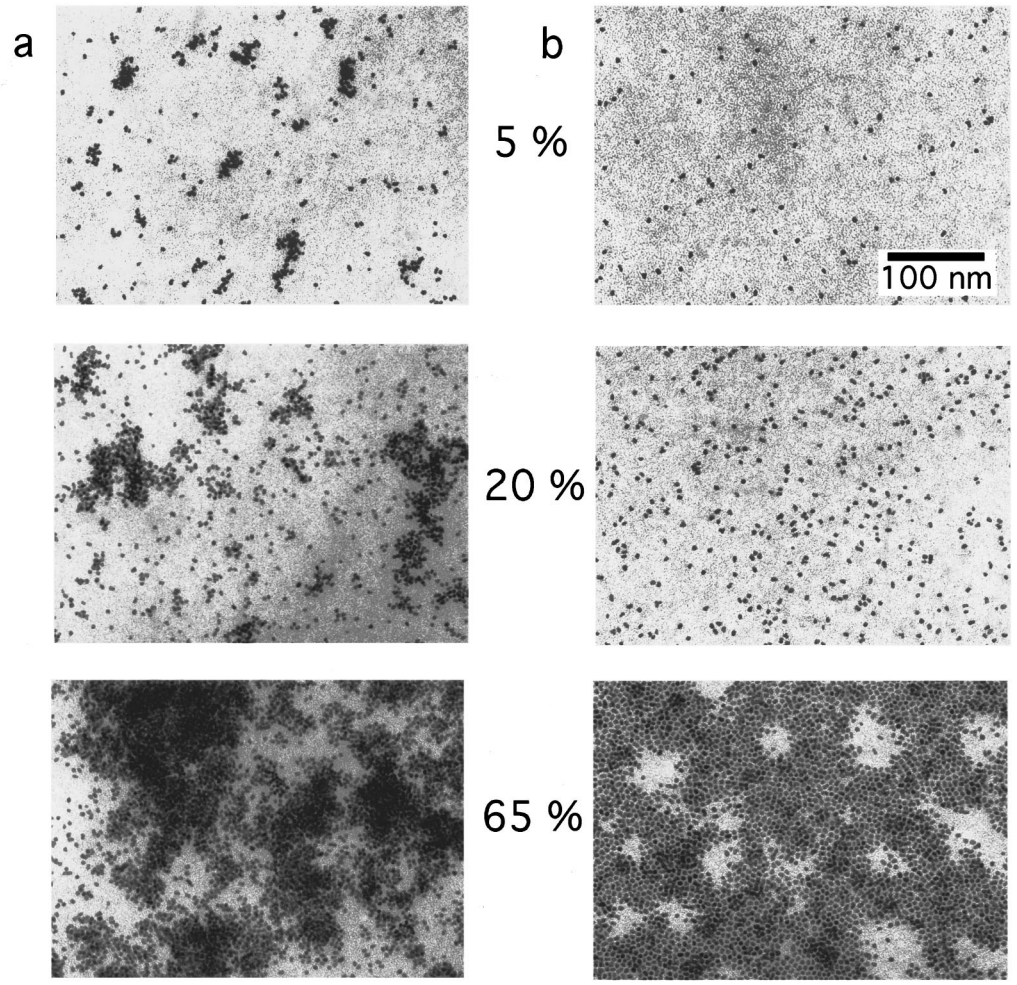

FIG. 6. TEM images of blends of MEH-PPV with 5-nm-diameter CdSe nanocrystals at concentrations of 5%, 20%, and 65% by weight. (a) Pyridine-treated nanocrystals. (b) TOPO-coated nanocrystals. These images are taken on free-standing areas of the films. The polymer background is clearly visible, showing that the films are continuous.

action spectrum at 560 nm, on the rising edge of the polymer absorption spectrum, as has been described previously for this kind of device.[7] Due to the poor electron transport in the polymer, only those electrons generated close to the aluminum electrode will contribute to the photocurrent by reaching the electrode without recombination. The peak photocurrent therefore occurs where the optical density is low and light is absorbed throughout the thickness of the device, rather than at high optical densities where almost all the light is absorbed close to the ITO electrode. Similar behavior is seen in devices with low concentrations of CdSe. In contrast, at high concentrations of CdSe, the action spectrum closely follows the fraction of incident light absorbed in the device. This result indicates that both carriers are mobile within the composite material at high nanocrystal concentrations.

Figure 11 shows the temperature dependence of the photocurrent at 514 nm, between room temperature and 10 K. The heating and cooling curves show some hysteresis, which is repeatable on subsequent cycles. The photocurrent drops by only a factor of 5 between room temperature and 10 K, indicating that the limiting process in determining the photoconductivity is not strongly thermally activated.

IV. DISCUSSION

The photoluminescence data show that in blends of MEH-PPV and CdS or CdSe nanocrystals, excitons are dissociated at the polymer/nanocrystal interface, leaving the electron on the nanocrystal and the hole on the polymer. The morphology of the composite nanocrystal/polymer materials is such that a large fraction of the excitons produced are dissociated at an interface, even at relatively low nanocrystal concentrations. The presence of a TOPO surface layer on the nanocrystal, however, suppresses the charge transfer process. The photoconductivity action spectra show that both absorption in the polymer and absorption in the nanocrystal lead to charge separation.

As discussed in the Introduction, efficient photoconductivity requires not only efficient charge separation, but also efficient transport of the carriers to the electrodes without recombination. Recombination is minimized when the carriers are separated onto different materials, and both carriers have pathways to the appropriate electrode within the component of the film onto which they have been separated. It can be seen from Fig. 6(a) that at low concentrations of

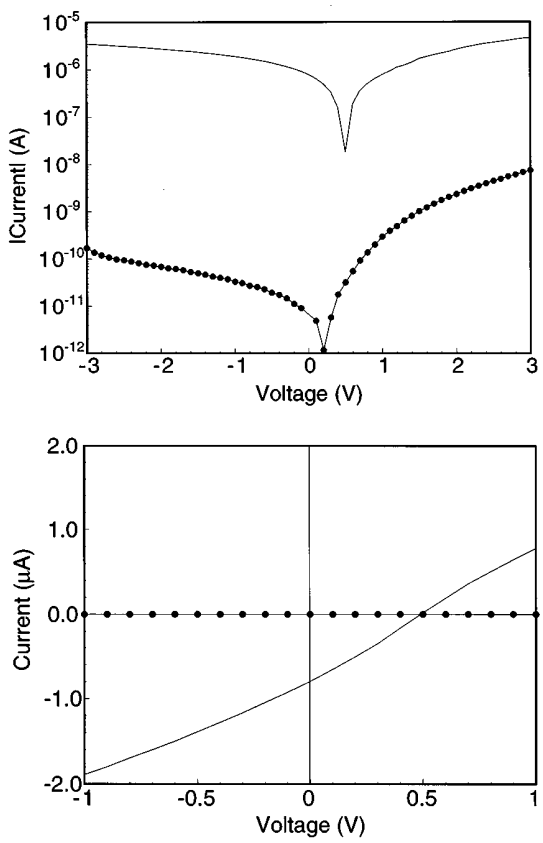

FIG. 7. (a) Current-voltage curve for a device containing 90 wt % CdSe in the dark (circles) and under illumination at 514 nm (solid line). The active area of the device was 7.3 mm^2, and the illumination was from a laser spot which was contained within the active area. The maximum power density of the illumination was approximately 5 $W\,m^{-2}$. (b) Shows the same data for a smaller range of voltage, with the current on a linear axis.

nanocrystals the size of the nanocrystal domains is small, so only the few electrons generated on the larger nanocrystal domains very close to the aluminum electrode will have a pathway to the electrode. At higher concentrations [see Fig. 6(a), with a concentration of 65 wt % nanocrystals], the nanocrystals begin to form a connected network. In this case, it becomes much more likely for an electron generated on a nanocrystal at a general position within the device to be able to find its way through the thickness of the device. It should be noted that the direction of transport in the devices is of course perpendicular to the plane shown in the TEM images, and that the films used for the TEM images are much thinner than those used for devices. Nevertheless, there is clear evidence of stacking of the nanocrystals within the thin TEM films in such a way as to allow perpendicular transport, and we believe that the morphology within the plane of the thin films is a useful indication of the likely morphology affecting the transport in the perpendicular direction.

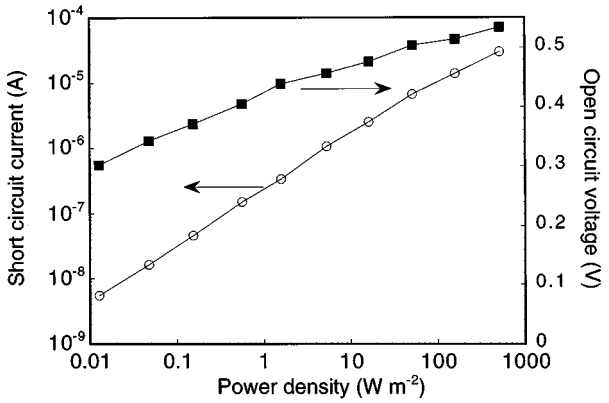

FIG. 9. Short-circuit current (circles) and open-circuit voltage (squares) as a function of incident light intensity for a device containing 90 wt % of 5-nm-diameter CdSe nanocrystals. Excitation was from an argon ion laser at 514 nm. The beam profile was approximately Gaussian, with a full width at half maximum of 1.4 mm. The intensity shown is the approximate maximum intensity at the center of the laser spot.

It is important to distinguish here between the effects of charge separation and the effects of transport. At 40 wt % of nanocrystals, for example, the PL is quenched by a factor of approximately 10. In the presence of the internal field within the device, it is therefore likely that significantly more than

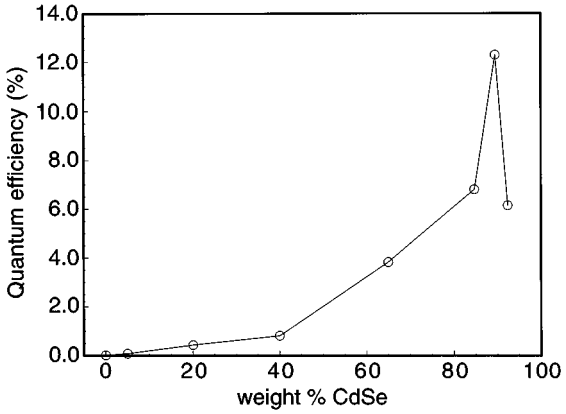

FIG. 8. Short-circuit quantum efficiency for devices containing 5-nm-diameter CdSe nanocrystals, as a function of CdSe concentration. Excitation was at 514 nm, at a power density of approximately 5 $W\,m^{-2}$.

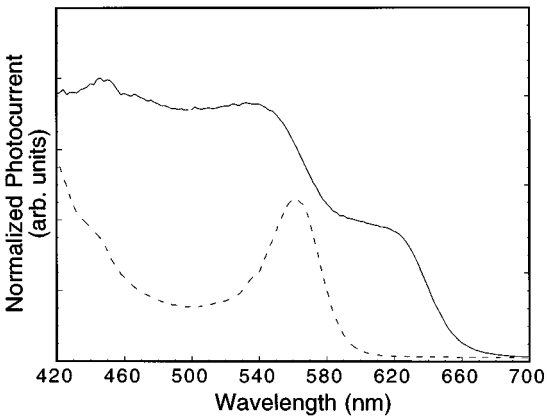

FIG. 10. Spectral response of the short circuit current for a device containing 90 wt % 5-nm-diameter CdSe nanocrystals (solid line), and for a pure MEH-PPV device (dashed line). The data have been normalized to fit on the same scale.

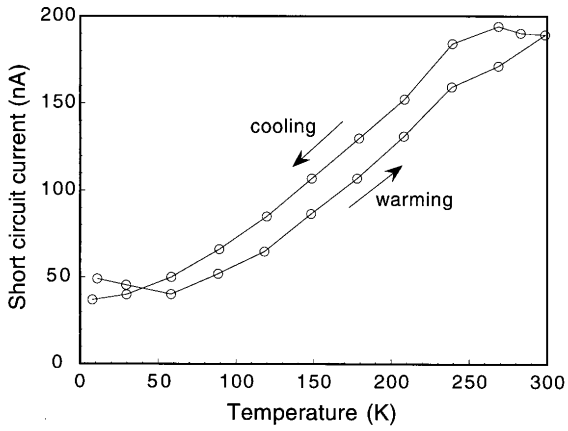

FIG. 11. Temperature dependence of the short circuit current for a device containing 90 wt % 5-nm-diameter CdSe nanocrystals, for warming followed by cooling. The device was allowed to equilibrate for several minutes at each temperature before the measurement was taken.

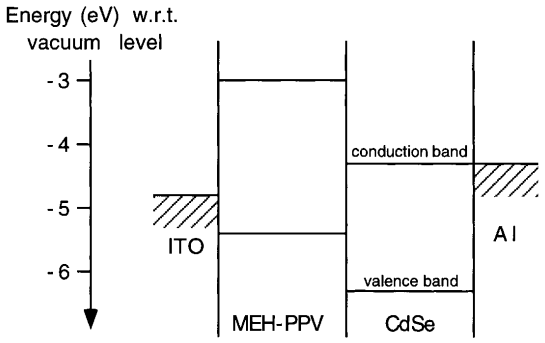

FIG. 12. Energy level diagram for an ITO/MEH-PPV:CdSe/Al device, for a CdSe nanocrystal diameter of 5 nm. As discussed in the text, the exact ionization potentials for the various materials shown here are not accurately known; however, this diagram gives a useful indication of relative positions.

90% of the excitons are dissociated at an interface. Although the short-circuit quantum efficiency of this device is much larger than that of a pure MEH-PPV device, it is still more than a factor of 10 smaller than the maximum efficiency found in the device with 90 wt % CdSe. We therefore conclude that the improvement in efficiency between 40 and 90 wt % is largely due to improvement in electron transport, and that the improvement in efficiency at lower concentrations is due to improvements in both charge separation and transport. The peak in efficiency at 90 wt % CdSe corresponds to a volume fraction of nanocrystal of approximately 65%, at which point there should be good percolation paths through both nanocrystal and polymer components. (The true volume percentages of nanocrystal are less than the fraction of dark area in the TEM images, since the TEM films are thicker than one nanocrystal diameter.)

Even at the optimum concentration of nanocrystals, the photocurrent quantum efficiency is less than unity. We propose that the loss of carriers is largely due to electrons which become trapped at ''dead ends'' in the nanocrystal network, from where they cannot hop to another nanocrystal in the direction of the internal field. These electrons will eventually recombine with holes in the neighboring polymer. This mechanism is consistent with the almost linear intensity dependence of the photocurrent observed at low intensities. A linear intensity dependence is characteristic of recombination at a fixed number of recombination centers. In contrast, bimolecular recombination of free electrons and holes would give an intensity dependence $I_{sc} \propto F^{0.5}$. The local field generated by an electron trapped at a dead end will tend to repel other electrons from taking this route, causing each dead end to act as a recombination center that can be either singly occupied or empty. This model is also consistent with the weak temperature dependence of the photocurrent, since the probability of recombination is determined largely by the morphology of the film, hence the exact rates of transport and recombination at a polymer/nanocrystal interface only have a secondary effect on the measured current.

In order to study the effect of the nanocrystal size on the photoconductivity, we have also studied devices using pyridine-treated CdSe nanocrystals of 2.4 nm diameter (absorption peak at 516 nm). These smaller nanocrystals also gave a significant improvement in photoconductivity, although the peak efficiencies reached were not as high as with the larger nanocrystals. At 81 wt % CdSe, for example, the quantum efficiency at 514 nm was 0.9%, compared with 5.5% for the larger nanocrystals. TEM images show that the typical size of nanocrystal domains is smaller than for the larger nanocrystals, probably as a result of improved solubility of the smaller particles. We attribute the lower efficiency to the reduced probability of electrons having a pathway to the aluminum electrode.

The low quantum efficiencies found using TOPO-coated nanocrystals are primarily a consequence of the fact that charge transfer is slow compared to the natural decay of excitons produced in either the polymer or the nanocrystals. The fact that the quantum efficiencies with TOPO-coated nanocrystals are even lower than those of pure MEH-PPV devices suggests that any free electrons which are produced by the internal field in the device become trapped on the nanocrystals, and that the presence of the TOPO barrier inhibits transport from nanocrystal to nanocrystal before recombination occurs. This evidence for poor transport between TOPO-coated nanocrystals may be relevant to explain the performance of light-emitting diodes fabricated from layers of TOPO-coated CdSe nanocrystals.[33]

Figure 12 shows a schematic energy level diagram for an ITO/MEH-PPV:CdSe/Al device, assuming that both semiconductors act as intrinsic materials. The ionization potential and electron affinity of 5-nm-diameter CdSe nanocrystals were estimated from the bulk values,[35] assuming that 75% of the shift due to quantum confinement occurs in the conduction band. The values for MEH-PPV are taken from Ref. 36 although a range of values are quoted in the literature. Since the work function of ITO is smaller than the ionization potential of MEH-PPV and the work function of Al close to the electron affinity of CdSe nanocrystals, the expected maximum open circuit voltage is given by the difference in work function between ITO (4.7–4.9 eV) and Al (4.3 eV). The open-circuit voltages of the devices studied depended on the excitation intensity, and also showed some variation from device to device, but were typically in the range 0.5–0.6 eV at intensities above 5 W m^{-2}. These values are consistent

with the difference in work functions between Al and ITO. We do not see a significant increase in the open-circuit voltage when using 2.4-nm-diameter nanocrystals. This result is as expected since the conduction band of these nanocrystals lies above the work function of Al. We anticipate that larger open circuit voltages could be achieved using small nanocrystals with low work function electrodes.

Although the primary interest of this paper is to investigate the physical processes of charge separation and transport in composite polymer/nanocrystal materials, it is useful for comparison to other work on photovoltaic materials to calculate the energy conversion efficiency for the devices studied here. The device described in Fig. 7 has a quantum efficiency of 12% at 514 nm. This value is significantly larger than values of 2–6 % reported for polymer/polymer mixtures,[14,15] but not as large as the value of approximately 36% found at this excitation intensity in blends of derivatized C_{60} and MEH-PPV.[21] In the devices studied here, the fill factor [defined as $(VI)_{max}/V_{oc}I_{sc}$, where $(VI)_{max}$ is the area of the largest rectangle under the current-voltage curve between 0 V and V_{oc}] is 0.26, and the open-circuit voltage is approximately 0.5 V, giving a power conversion efficiency of 0.6% at 514 nm. The device begins absorbing at 650 nm, and thus covers a wider spectral range than devices where absorption occurs solely in MEH-PPV. For the solar spectrum under AM 1.5 conditions (a typical solar spectrum), the device absorbs approximately 37% of the incident solar energy, and the energy conversion efficiency for AM 1.5 conditions at 5 $W\,m^{-2}$ is 0.2%. Due to the sublinear intensity dependence of the photocurrent, under one-sun conditions (800 $W\,m^{-2}$) the solar power conversion efficiency will be approximately 0.1%. For comparison, we estimate that the solar energy conversion efficiency for devices using blends of derivatized C_{60} and MEH-PPV with calcium electrodes[21] is no more than 0.5% under the same conditions. We have identified above the possibility of increasing the open-circuit voltage, and hence the power efficiency, by using smaller nanocrystals with lower work-function electrodes. Further understanding of the injection and transport of carriers of these devices may in the future allow improved fill factors to be obtained.

V. CONCLUSIONS

We have demonstrated that the interface between a conjugated polymer and a semiconductor nanocrystal can be used to provide efficient charge separation for neutral excited states produced either on the polymer or on the nanocrystal. We have also shown that both charge separation and charge transport from nanocrystal to nanocrystal are suppressed in the presence of a TOPO surface layer on the nanocrystal. The morphology of composite nanocrystal/polymer films shows phase separation of the polymer and nanocrystal components. In photovoltaic devices using the composite materials, this phase segregation is crucial in providing paths for both electrons and holes to travel to the appropriate electrode without recombination. The use of nanocrystals allows great flexibility in controlling the performance of photovoltaic devices, since both the electronic energy levels and the morphology of the composite materials may be altered by changing the nanocrystal size, concentration, and surface ligand. We have shown how the absorption range of polymer devices can be widened by the incorporation of nanocrystals, and using transmission electron microscopy we have directly demonstrated the relationship between film morphology and photovoltaic performance. We have shown that large improvements in photovoltaic efficiency can be achieved by using high concentrations of nanocrystals, and we anticipate that further improvements will be made in the future using the principles developed here to optimize the charge transport process.

ACKNOWLEDGMENTS

This work was supported by the U.S. Department of Energy under Contract No. DE-AC0376SF00098. N.C.G. thanks the Miller Institute for Basic Research in Science for support. We are grateful to M. Shtein for assistance with the experimental work. The TEM work was carried out in the Robert D. Ogg Electron Microscope Laboratory, University of California, Berkeley.

*Present address: Cavendish Laboratory, Madingley Road, Cambridge, CB3 OHE, U.K.

[1] N. C. Greenham and R. H. Friend, in *Solid State Physics*, edited by H. Ehrenreich and F. Spaepen (Academic, San Diego, 1995), Vol. 49, p. 1.

[2] J. H. Burroughes, D. D. C. Bradley, A. R. Brown, R. N. Marks, K. Mackay, R. H. Friend, P. L. Burn, and A. B. Holmes, Nature **347**, 539 (1990).

[3] D. Braun and A. J. Heeger, Appl. Phys. Lett. **58**, 1982 (1991).

[4] G. Grem, G. Leditzky, B. Ullrich, and G. Leising, Adv. Mater. **4**, 36 (1992).

[5] N. C. Greenham, S. C. Moratti, D. D. C. Bradley, R. H. Friend, and A. B. Holmes, Nature **365**, 628 (1993).

[6] S. Karg, W. Reiss, V. Dyakonov, and M. Schwoerer, Synth. Met. **54**, 427 (1993).

[7] R. N. Marks, J. J. M. Halls, D. D. C. Bradley, R. H. Friend, and A. B. Holmes, J. Phys. Condens. Matter **6**, 1 (1994).

[8] H. Antoniadis, B. R. Hsieh, M. A. Abkowitz, S. A. Jenekhe, and M. Stolka, Synth. Met. **62**, 265 (1994).

[9] G. Yu, C. Zhang, and A. J. Heeger, Appl. Phys. Lett. **64**, 1540 (1994).

[10] K. Yoshino, X. H. Yin, K. Muro, S. Kiyomatsu, S. Morita, A. A. Zakhidov, T. Noguchi, and T. Ohnishi, Jpn. J. Appl. Phys. **32**, L357 (1993).

[11] N. S. Sariciftci, D. Braun, C. Zhang, V. I. Srdanov, A. J. Heeger, G. Stucky, and F. Wudl, Appl. Phys. Lett. **62**, 585 (1993).

[12] G. Yu, K. Pakbaz, and A. J. Heeger, Appl. Phys. Lett. **64**, 1 (1994).

[13] J. J. M. Halls, K. Pichler, R. H. Friend, S. C. Moratti, and A. B. Holmes, Appl. Phys. Lett. **68**, 3120 (1996).

[14] J. J. M. Halls, C. A. Walsh, N. C. Greenham, E. A. Marseglia, R. H. Friend, S. C. Moratti, and A. B. Holmes, Nature **376**, 498 (1995).

[15] G. Yu and A. J. Heeger, J. Appl. Phys. **78**, 4510 (1995).

[16] R. A. J. Janssen, M. P. T. Christiaans, C. Hare, N. Martin, N. S. Sariciftci, A. J. Heeger, and F. Wudl, J. Chem. Phys. **103**, 8840 (1995).

[17] K. E. Ziemelis, A. T. Hussain, D. D. C. Bradley, R. H. Friend, J. Rühe, and G. Wegner, Phys. Rev. Lett. **66**, 2231 (1991).
[18] P. Dyreklev, O. Inganäs, J. Paloheimo, and H. Stubb, J. Appl. Phys. **71**, 2816 (1992).
[19] P. J. Hamer, K. Pichler, M. G. Harrison, R. H. Friend, B. Ratier, A. Moliton, S. C. Moratti, and A. B. Holmes, Philos. Mag. B **73**, 367 (1996).
[20] L. Smilowitz, N. S. Sariciftci, R. Wu, C. Gettinger, A. J. Heeger, and F. Wudl, Phys. Rev. B **47**, 13 835 (1993).
[21] G. Yu, J. Gao, J. C. Hummelen, F. Wudl, and A. J. Heeger, Science **270**, 1789 (1995).
[22] M. G. Bawendi, M. L. Steigerwald, and L. E. Brus, Annu. Rev. Phys. Chem. **41**, 477 (1990).
[23] A. P. Alivisatos, Science **271**, 933 (1996).
[24] T. Vossmeyer, L. Katsikas, M. Giersig, I. G. Popovic, K. Diesner, A. Chemseddine, A. Eychmuller, and H. Weller, J. Phys. Chem. **98**, 7665 (1994).
[25] B. O'Regan and M. Grätzel, Nature **353**, 737 (1991).
[26] Y. Wang and N. Herron, Chem. Phys. Lett. **200**, 71 (1992).
[27] B. O. Dabbousi, M. G. Bawendi, O. Onitsuka, and M. F. Rubner, Appl. Phys. Lett. **66**, 1316 (1995).
[28] C. B. Murray, D. J. Norris, and M. G. Bawendi, J. Am. Chem. Soc. **15**, 8706 (1993).
[29] J. E. B. Katari, V. L. Colvin, and A. P. Alivisatos, J. Phys. Chem. **98**, 4109 (1994).
[30] N. C. Greenham, I. D. W. Samuel, G. R. Hayes, R. T. Phillips, Y. A. R. R. Kessener, S. C. Moratti, A. B. Holmes, and R. H. Friend, Chem. Phys. Lett. **241**, 89 (1995).
[31] L. Smilowitz, A. Hays, A. J. Heeger, G. Wang, and J. E. Bowers, J. Chem. Phys. **98**, 6504 (1993).
[32] I. D. W. Samuel, B. Crystal, G. Rumbles, P. L. Burn, A. B. Holmes, and R. H. Friend, Chem. Phys. Lett. **213**, 472 (1993).
[33] V. L. Colvin, M. C. Schlamp, and A. P. Alivisatos, Nature **370**, 354 (1994).
[34] J. J. Shiang, A. V. Kadavanich, R. K. Grubbs, and A. P. Alivisatos, J. Phys. Chem. **99**, 17 417 (1994).
[35] T. C. Chiang and F. J. Himpsel, *Electronic Structure of Solids*, Landolt-Börnstein, New Series, Group III, Vol. 23, Pt. 2 (Springer, Berlin, 1989).
[36] I. H. Campbell, T. W. Hagler, and D. L. Smith, Phys. Rev. Lett. **76**, 1900 (1996).